Original Article
Yonsei Med J 2025 Apr;66(4):249-258
https://doi.org/10.3349/ymj.2024.0082
Yonsei Medical Journal
YMJ
pISSN: 0513-5796 · eISSN: 1976-2437

Prospective Evaluation of Various Ultrasound Parameters for Assessing Renal Allograft Rejection Subtypes: Elasticity and Dispersion as Diagnostic Tools

Yeji Kwon[1], Jongjin Yoon[1], Dae Chul Jung[1], Young Taik Oh[1], Kyunghwa Han[1], Minsun Jung[2], and Byung Chul Kang[1]

Departments of [1]Radiology and [2]Pathology, Severance Hospital, Yonsei University College of Medicine, Seoul, Korea.

Purpose: Renal allograft rejection, either acute or chronic, is prevalent among many recipients. This study aimed to identify multiple Doppler ultrasound parameters for predicting renal allograft rejection.

Materials and Methods: Between November 2021 and April 2022, 61 renal allograft recipients were studied prospectively after excluding two patients with dual transplants and seven with hydronephrosis. The analysis excluded 11 cases (10 due to missing Doppler data or pathology reports and one due to a high interquartile range/median dispersion value), resulting in a final analysis of 50 patients. Clinical characteristics, color Doppler imaging, superb microvascular imaging, and shear-wave imaging parameters were assessed by three experienced genitourinary radiologists. The Banff classification of the biopsy tissue served as the reference standard. Univariable and multivariable logistic regression, contingency matrices, and multiple machine-learning models were employed to estimate the associations.

Results: Fifty kidney transplant recipients (mean age, 53.26±8.86 years; 29 men) were evaluated. Elasticity (≤14.8 kPa) demonstrated significant associations for predicting the combination of (borderline) T cell-mediated rejection (TCMR) categories (Banff categories 3 and 4) (p=0.006) and yielded equal or higher area under the receiver operating characteristics curve (AUC) values compared to various classifiers. Dispersion (>15.0 m/s/kHz) was the only significant factor for predicting the combination of non-TCMR categories (Banff categories 2, 5, and 6) (p=0.026) and showed equal or higher AUC values than multiple machine learning classifiers.

Conclusion: Elasticity (≤14.8 kPa) showed a significant association with the combination of (borderline) TCMR categories, whereas dispersion (>15.0 m/s/kHz) was significantly associated with the combination of non-TCMR categories in renal allografts.

Key Words: Renal allograft rejection, color doppler imaging, shear-wave imaging, elasticity, dispersion

INTRODUCTION

Kidney transplantation is regarded as the optimal treatment for patients with end-stage renal disease.[1] With considerable advancements in immunosuppressive protocols and surgical techniques, the short-term results of renal allografts have significantly improved, with the rejection rate now being less than 15%.[2] However, despite advancements in immunosuppressive therapy, a significant proportion of renal allografts experience rejection, an immunological reaction to donor antigens recognized by the recipient's immune system.[3] Therefore, accurate and timely detection, as well as the classification of pathologic subtypes of graft rejection, is crucial for appropriate management and improved survival of renal allografts.

Renal allograft biopsy has been widely used as a standard reference tool for diagnosing and classifying renal allograft rejection.[4] However, a biopsy is an invasive procedure with low

Received: April 25, 2024 **Revised:** September 5, 2024
Accepted: September 20, 2024 **Published online:** January 21, 2025
Corresponding author: Byung Chul Kang, MD, PhD, Department of Radiology, Severance Hospital, Yonsei University College of Medicine, 50-1 Yonsei-ro, Seodaemun-gu, Seoul 03722, Korea.
E-mail: kangbchwangsj@yuhs.ac

•The authors have no potential conflicts of interest to disclose.

risk of complications; the overall complication rate can be up to 8.7%.[5] Moreover, it may not be practical for frequent monitoring. Therefore, a need exists for non-invasive alternatives to biopsy, and clinicians have investigated alternative non-invasive methods that could wholly or partially replace renal allograft biopsy.

Multiparametric ultrasound has been widely utilized as a non-invasive tool for evaluating the status of renal allografts. Besides conventional brightness (B)-mode imaging, color Doppler ultrasound has been employed as a valuable tool by measuring the resistance index (RI), despite the ongoing controversy regarding the predictive value of RI (RI >0.8 has hazard ratios of 5.2, 2.14, and 3.46 for predicting renal allograft rejection at 3, 12, and 24 months, respectively).[6] Recently, various techniques, such as shear-wave imaging (SWI),[7] superb microvascular imaging (SMI),[8] and contrast-enhanced ultrasound (CEUS),[9] have been suggested as predictive parameters of renal allograft rejection (the AUROC for predicting renal allograft rejection is 0.80 for SWI and 0.94 for CEUS; there is controversy regarding the predictive value of SMI). Additionally, CEUS requires the use of contrast media and has a very long examination time.

Although various ultrasound parameters have been investigated as predictive factors for renal allograft rejection, no attempts have been made to predict rejection subtypes based on pathology. The Banff classification of allograft pathology is the most widely used standardized classification for categorizing the pathologic subtypes of renal allografts.[10] T cell-mediated rejection (TCMR) and antibody-mediated rejection, as defined by the Banff classification, require different treatment approaches, such as anti-thymocyte globulin treatment and plasmapheresis, respectively.[11] Therefore, the development of non-invasive ultrasound parameters that can differentiate specific subtypes of renal allograft rejection is essential to facilitate timely and appropriate therapeutic interventions. To the best of our knowledge, no ultrasound-based study has distinguished between the pathological subtypes of renal allograft rejection. Consequently, this study aimed to prospectively investigate the utility of multiple ultrasound parameters, including B-mode imaging, two-dimensional (2D) SWI, and SMI, in distinguishing the subtypes of renal allograft rejection in patients with clinically suspected graft rejection.

MATERIALS AND METHODS

Study population

This single-center prospective study was approved by the Institutional Review Board (IRB) (4-2021-0769). Between November 2021 and April 2022, 61 renal allograft recipients at Severance Hospital were enrolled in the study. All patients provided informed consent before participation. The study protocol conformed to the ethical guidelines of the 1975 Declaration of Helsinki.

The enrolled patients underwent Doppler ultrasound and subsequent renal allograft biopsy as part of the posttransplant evaluation process. The inclusion criteria were as follows: 1) age of 18 years or older; 2) single functioning renal allograft; 3) on immunosuppressant therapy; and 4) clinically suspected graft rejection [increased serum creatinine (Cr) ≥1.1 mg/dL] or decreased estimated glomerular filtration rate (eGFR) (<60 mL/min/1.73m^2), positive donor-specific antibodies, and suspected viral infection (blood BK virus quantitative polymerase chain reaction >4500 copies/mL). Patients were excluded if they had 1) malignant tumors or metastases (n=0); 2) undergone two transplants (n=2); 3) a history of severe allograft damage (n=0); 4) hydronephrosis (n=7); or 5) peri-transplant collection (n=0). Ineligible biopsy criteria were as follows: 1) absence of pathology results (n=2); 2) not measured elasticity (n=7); 3) not measured SMI-vascular index (SMI-VI) (n=1); and 4) interquartile range (IQR)/median of dispersion >0.4 (n=1), set to ensure data reliability, considering the sample size and the heterogeneous nature of the renal parenchyma (Fig. 1).[12,13]

Data collection and ultrasound measurements

Data on clinical characteristics, such as age, sex, medical history, weight, height, the time interval between biopsy and transplantation date, serum Cr level, and eGFR, were collected for

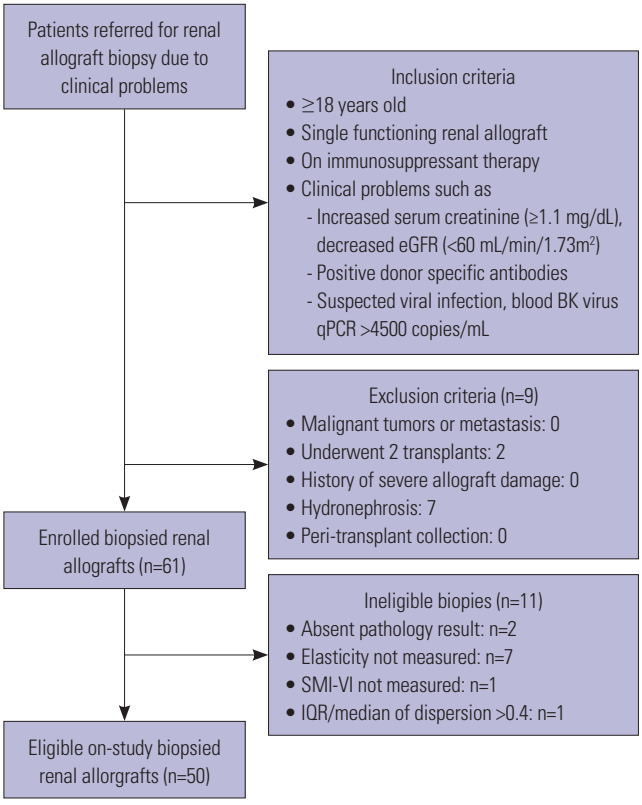

Fig. 1. Flowchart of the study population. eGFR, estimated glomerular filtration rate; qPCR, quantitative polymerase chain reaction; SMI-VI, superb microvascular imaging-vascular index.

https://doi.org/10.3349/ymj.2024.0082

each patient.

A commercial scanner (Aplio i800; Canon Medical Systems Corp., Otawara, Japan) was equipped with a convex PVI-475BX (1–8 MHz) probe, and the graft was evaluated using ultrasound. The patients were scanned in the supine position. On grayscale ultrasound examination, renal allografts were assessed for various parameters, including their length, parenchymal thickness, distance from the epidermis, echogenicity, as well as the existence of hydronephrosis, stones, or tumors. On color Doppler ultrasound examination, both the RI, calculated as (peak systolic velocity–diastolic velocity)/peak systolic velocity, and the pulsatility index (PI), calculated as (peak systolic velocity–minimal diastolic velocity)/mean velocity, were measured. These measurements were taken at the interlobar artery level within the renal allograft at a minimum of three different locations: the upper, middle, and lower poles, and the average RI and PI values were recorded.

Following the grayscale and color Doppler ultrasound assessments, 2D shear-wave elastography (2D-SWE) was employed to evaluate the tissue elasticity of the renal allograft. In addition to the conventional B-mode image, the system also presented a color-coded map to show the spatial distribution of elasticity values within the acquisition box. According to the manufacturer's recommended measurement protocol, a region of interest (ROI) with a 7-mm diameter should be placed in the area featuring the most parallel propagation contours, ideally at the upper portion of the acquisition box. After calculating the slope of the 2D shear-wave dispersion (2D-SWD) curve, the ultrasound system generated a single, SWD-related metric and presented both the average SWD (m/s/kHz) and the standard deviation pertaining to the selected ROI. In this study, 2D-SWE and 2D-SWD were performed four times in each cortex, and the mean values were used for statistical analyses. All ultrasound examinations were performed by three faculty genitourinary radiologists (B.C.K., D.C.K., and Y.T.O., with 27, 18, and 21 years of genitourinary faculty experience, respectively), with each patient being examined by one radiologist. During data collection, radiologists remained unaware of patients' clinical details, ensuring an unbiased perspective.

Renal allograft biopsy

Under ultrasound guidance, three faculty genitourinary radiologists performed percutaneous renal allograft biopsy with an 18-gauge semiautomatic biopsy instrument (Medax Velox 2). Each biopsy involved the collection of three to four specimens. The biopsy results were evaluated based on the Banff classification 2019.[14]

Pathologic analysis

Pathologic findings were evaluated by a pathologist (M.S.J.) at Severance Hospital. The Banff classification 2019 was used as the reference standard for assessing renal allograft rejection. Based on this classification, renal allograft rejection was evaluated and classified into six distinct categories: category 1, normal biopsy or nonspecific changes; category 2, antibody-mediated changes; category 3, suspicious (borderline) for acute TCMR; category 4, TCMR; category 5, interstitial fibrosis and tubular atrophy; and category 6, other changes not considered to be caused by acute or chronic rejection.[15]

Construction of clinical models

Prior to developing clinical models, an initial visual examination of the data was performed using two techniques for dimensionality reduction: Principal Component Analysis (PCA) and t-distributed Stochastic Neighbor Embedding (t-SNE).[16]

Clinical models for predicting the combination of borderline acute TCMR and TCMR categories and the combination of non-TCMR categories were developed using logistic regression (LR), decision tree (DT),[17] random forest (RF),[18] support vector machine (SVM),[19] linear discriminant analysis (LDA),[20] and Gaussian Naïve Bayes (GNB).[21] The entire sample was randomly split into a 7:3 ratio, designating the subsets as training and test sets, respectively. The hyperparameters used for training each model are summarized in Supplementary Table 1 (only, online). Python (version 3.8.3; Python Software Foundation, Wilmington, DE, USA), Visual Studio Code (version 1.67; Microsoft Corporation, Redmond, WA, USA), and Scikit-learn (version 1.0.2) were used to conduct machine learning analysis.

Evaluation metrics

The performance of the proposed model for predicting the combination of borderline acute TCMR and TCMR categories and the combination of non-TCMR categories was evaluated using the area under the receiver operating characteristics curve (AUC), confusion matrix, accuracy (ACC), true positive rate (TPR), true negative rate (TNR), false positive rate (FPR), false negative rate (FNR), positive prediction value (PPV), negative prediction value (NPV), and false discovery rate (FDR).

Statistical analysis

Univariable and multivariable LR analyses were used to examine the associations between the clinical and Doppler parameters, the combination of borderline acute TCMR and TCMR, and the combination of non-TCMR. Variables with $p<0.05$ in the univariable analysis were then entered into the multivariable analysis. For multivariable analysis, a stepwise backward elimination method (backward:conditional) was used. The Mann–Whitney U test was used for continuous variables, and χ^2 or Fisher's exact test was used for categorical variables. ROC curves were generated, and Youden's Index (J) was used to find the optimal cutoff points for elasticity and dispersion. Interobserver variability was evaluated using the analysis of variance (ANOVA) method, where one radiologist independently measured results for one patient. Statistical analyses were performed using SPSS (version 23.0; IBM Corp., Armonk, NY,

USA). Statistical significance was set at $p<0.05$.

RESULTS

Study patient characteristics

Fifty kidney transplant recipients (mean age, 53.26±8.86 years; 29 men and 21 women) with clinically suspected graft rejection were included in this study. The demographic and clinical characteristics of the study participants are shown in Table 1. Sixteen (32.0%) patients were classified as Banff category 5, whereas the remaining five categories were distributed within the range of 10.0%–14.0%. The serum Cr level was elevated (1.72 [1.50, 2.90] mg/dL), and the eGFR was decreased (34.93 [23.25, 45.00] mL/min/1.73m^2) compared to the normal range. The median time interval between kidney transplantation and biopsy was 166.50 days.

Table 1. Demographic, Laboratory, Sonographic, and Pathologic Characteristics of Study Patients (n=50)

Parameters	Value
Age (yr)	53.26 [48.00, 60.00]
Sex	
Men	29 (58)
Women	21 (42)
BMI (kg/m^2)	22.36 [20.24, 24.08]
Hypertension	44 (88)
Diabetes mellitus	20 (38)
Biopsy-transplant interval (days)	166.50 [34.75, 4264.25]
Serum creatinine (mg/dL)	1.72 [1.50, 2.90]
eGFR (mL/min/1.73m^2)	34.93 [23.25, 45.00]
Sonographic parameters	
Graft length (cm)	11.02 [10.30, 11.58]
Parenchymal thickness (mm)	18.50 [17.00, 22.23]
PSI	1.79 [1.52, 2.02]
RI	0.71 [0.65, 0.82]
PI	1.38 [1.19, 1.49]
Vessel-to-capsule distance on Doppler (mm)	6.01 [4.10, 7.35]
Vessel-to-capsule distance on SMI (mm)	1.20 [0.50, 1.60]
SMI-VI (%)	24.32 [20.07, 28.91]
Elasticity (kPa)	19.92 [12.13, 25.78]
Dispersion (m/s/kHz)	13.75 [11.57, 18.78]
Banff category of biopsies	
1 (Normal biopsy or non-specific changes)	7 (14)
2 (Antibody-mediated changes)	9 (18)
3 (Suspicious for acute T cell-mediated rejection)	5 (10)
4 (T cell-mediated rejection)	6 (12)
5 (Interstitial fibrosis and tubular atrophy)	16 (32)
6 (Other non-rejection changes)	7 (14)

BMI, body mass index; eGFR, estimated glomerular filtration rate; PSI, parenchyma size index; RI, resistance index; PI, pulsatility index; SMI-VI, superb microvascular imaging-vascular index.
Data are continuous variables, reported as means [interquartile range]. Unless otherwise indicated, data represent number of patients, with percentage in parentheses.

Interobserver variability

The consistency of the ultrasound parameter measurements obtained by the three genitourinary-specialized faculty radiologists was assessed using ANOVA. No significant differences were found in the measurements of SMI-VI, elasticity, and dispersion (p=0.751, 0.252, and 0.209, respectively), demonstrating a high degree of interobserver agreement (Fig. 2).

Elasticity as predictive factor for the combination of borderline acute TCMR and TCMR categories

To evaluate the categories related to TCMR, we tried to develop a predictive model by combining borderline acute TCMR and TCMR (categories 3 and 4, n=11). Examples of ultrasound images for TCMR and non-TCMR categories are shown in Fig. 3. Results of univariable analysis and χ^2-test of clinical parameters for the combination of borderline acute TCMR and TCMR categories are summarized in Table 2 and Supplementary Tables 2 and 3 (only online). Patients in the combination group of borderline acute TCMR and TCMR categories exhibited lower elasticity (kPa) (12.4 vs. 22.1, p=0.002) and dispersion (m/s/kHz) (12.0 vs. 16.3, p=0.019). However, multiparametric ultrasound features, including graft length, parenchymal thickness, RI, PI, and vessel-to-capsule distance on Doppler and SMI images, showed no association with the combination of acute TCMR and TCMR categories. In the multivariable LR analysis, elasticity was the only significant predictor of the combination of borderline acute TCMR and TCMR categories [odds ratio (OR) 0.840, 95% confidence interval (CI) 0.742–0.951, p=0.006]. Supplementary Table 4 (only online) presents the sensitivity and specificity in predicting the combination of borderline acute TCMR and TCMR categories, with an elasticity threshold of ≤14.8 kPa showing a sensitivity of 90.91% and specificity of 76.92%.

Prior to utilizing machine-learning methods for building a clinical prediction model for the amalgamation of borderline acute TCMR and TCMR categories, the dataset underwent visual exploration using PCA and t-SNE techniques. No visually distinct clusters were observed (Supplementary Fig. 1, only online). Five machine-learning techniques (DT, RT, SVM, LDA, and GNB) were subsequently employed for model construction. Supplementary Fig. 2 (only online) illustrates the DT and the top six important features, with elasticity being the most significant, further emphasizing its high predictive value.

The ROC curves of the elasticity, DT, RT, SVM, LDA, and GNB models are shown in Fig. 4. The AUC was highest in the following order: elasticity (0.83), GNB (0.83), RF (0.78), SVM (0.75), DT (0.71), and LDA (0.64). Performance metrics of various machine learning classifiers are summarized in Supplementary Table 5 (only online). Notably, the AUC of elasticity demonstrated comparable or higher values than those of the other five machine learning models. Multiple performance metrics, in-

https://doi.org/10.3349/ymj.2024.0082

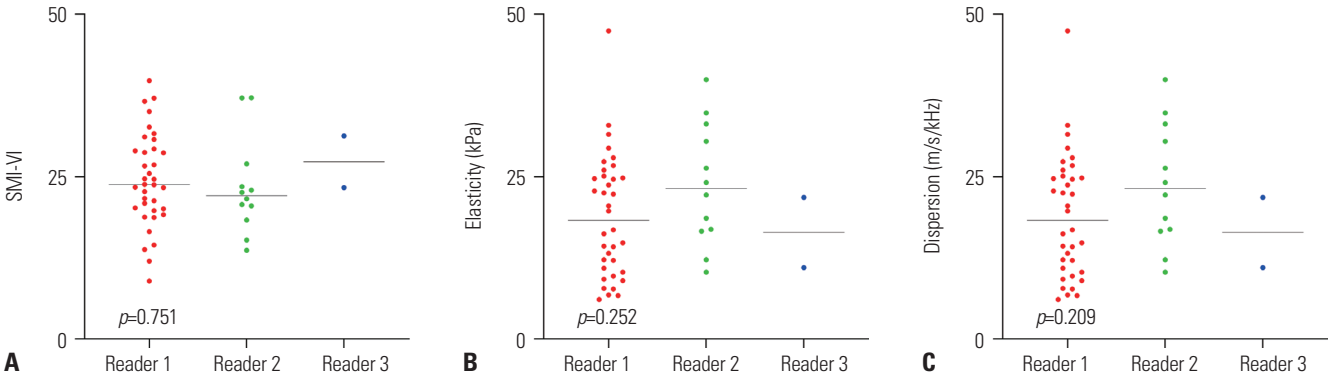

Fig. 2. Inter-reader agreement in SMI-VI (A), elasticity (B), and dispersion (C) measurement. SMI-VI, superb microvascular imaging-vascular index.

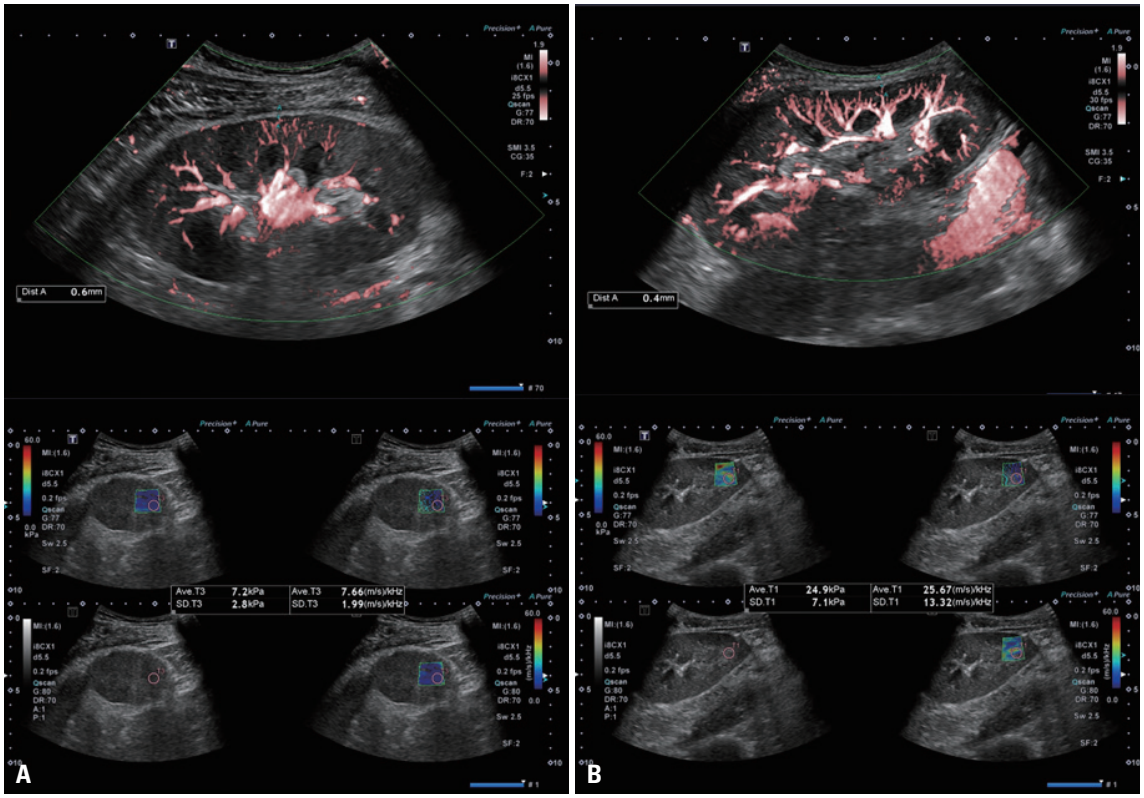

Fig. 3. Examples of ultrasound images for (A) TCMR and (B) non-TCMR. In SMI, SMI-VI and the distance from vessels to capsules were measured. In shear-wave imaging, elasticity, and dispersions were measured more than 5 times, and the average value was calculated. TCMR, T cell-mediated rejection; SMI-VI, superb microvascular imaging-vascular index.

cluding ACC, TPR, TNR, FPR, FNR, PPV, NPV, and FDR, for elasticity in predicting the combination of borderline acute TCMR and TCMR categories are shown in Table 3.

Dispersion as predictive factor for the combination of non-TCMR categories

To evaluate the categories related to non-TCMR, we tried to develop a predictive model by combining non-TCMR categories (categories 2, 5, and 6, n=32). Table 4 and Supplementary Tables 6 and 7 (only online) provide a summary of univariable analysis and χ^2-test of clinical parameters for the combination of non-TCMR categories. Patients in the combination group of non-TCMR showed higher dispersion (m/s/kHz) (16.7 vs. 13.1, p=0.018). However, multiparametric ultrasound features, including graft length, parenchymal thickness, RI, PI, vessel-to-capsule distance on Doppler and SMI images, and elasticity, were not associated with the combination of non-TCMR categories. In the multivariable LR analysis, only dispersion emerged as a significant predictor of the combination of non-TCMR categories (OR 1.175, 95% CI 1.019–1.355, p=0.026). The sensitivity and specificity of predicting the combination of non-TCMR categories based on dispersion are shown in Supplementary

Table 2. Univariable and Multivariable Binary Logistic Regression to Identify Ultrasound Parameters for Predicting the Combination of Borderline Acute TCMR (Banff Category 3) and TCMR (Banff Category 4)

	Univariable analysis		Multivariable analysis	
	OR (95% CI)	*p* value	OR (95% CI)	*p* value
Age	0.991 (0.919–1.069)	0.820		
Sex	0.739 (0.186–2.945)	0.669		
Height	1.012 (0.928–1.103)	0.789		
Weight	1.023 (0.951–1.099)	0.543		
BMI	1.063 (0.833–1.358)	0.622		
Hypertension	1.471 (0.153–14.091)	0.738		
Diabetes mellitus	2.143 (0.553–8.309)	0.270		
Serum creatinine	0.999 (0.695–1.436)	0.996		
eGFR	0.988 (0.947–1.030)	0.563		
RI	0.019 (0–10.583)	0.219		
PI	0.324 (0.055–1.906)	0.212		
Vessel to capsule distance (Doppler)	0.735 (0.524–1.031)	0.074		
Vessel to capsule distance (SMI)	1.219 (0.616–2.410)	0.570		
SMI-VI	0.962 (0.872–1.062)	0.446		
Elasticity (kPa)	0.840 (0.742–0.951)	0.006	0.840 (0.742–0.951)	0.006
IQR/median (elasticity)	4.339 (0–117610.7)	0.778		
Dispersion (m/s/kHz)	0.793 (0.644–0.975)	0.028		
IQR/median (dispersion)	0.046 (0–46.353)	0.383		
Graft length (cm)	0.550 (0.253–1.197)	0.132		
PT (mm)	1.090 (0.934–1.271)	0.274		
PSI	4.060 (0.735–22.427)	0.108		

TCMR, T-cell mediated rejection; OR, odds ratio; CI, confidence interval; BMI, body mass index; eGFR, estimated glomerular filtration rate; RI, resistance index; PI, pulsatility index; SMI-VI, superb microvascular imaging-vascular index; PT, parenchymal thickness; PSI, parenchyma size index.

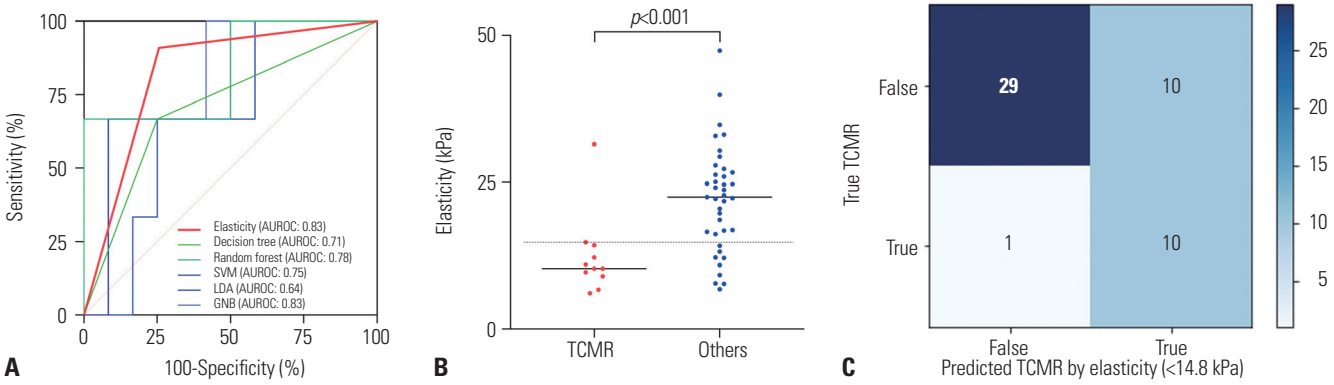

Fig. 4. (A) Receiver operating characteristic curves of elasticity (≤14.8 kPa) and multiple binary classifiers for predicting the combination of borderline acute TCMR (Banff category 3) and TCMR (Banff category 4). (B) A scatter plot for comparing the elasticity between the combination of borderline acute TCMR (Banff category 3) and TCMR (Banff category 4) groups and the remaining groups. (C) Contingency matrix of elasticity (≤14.8 kPa) and multiple binary classifiers for predicting the combination of borderline acute TCMR (Banff category 3) and TCMR (Banff category 4). TCMR, T-cell mediated rejection.

Table 8 (only online). Dispersion >15.0 m/s/kHz showed a sensitivity of 56.25% and a specificity of 94.44%.

Similar to the analysis conducted for the combination of acute TCMR and TCMR categories, the PCA and t-SNE analyses did not reveal visually distinct clusters (Supplementary Fig. 1, only online). Five machine-learning techniques (DT, RT, SVM, LDA, and GNB) were used to construct the clinical models. Supplementary Fig. 2 (only online) presents the DT and the top six important features, with elasticity being the most significant feature, followed by dispersion, contrary to the findings of the multivariable LR model.

Fig. 5 illustrates the ROC curves of the dispersion, DT, RT, SVM, LDA, and GNB models, with the AUC values ranked as follows: SVM (0.78), GNB (0.78), dispersion (0.75), LDA (0.74), DT (0.72), and RF (0.56). Performance metrics of various machine learning classifiers are summarized in Supplementary Table 9 (only online). The AUC of dispersion exhibited similar or slightly higher values than those of the other five machine

https://doi.org/10.3349/ymj.2024.0082

Table 3. Performance Metrics for the Elasticity (≤14.8 kPa) and Dispersion (>15.0 m/s/kHz) Used as Predictive Indicators for the Combination of Borderline Acute TCMR (Banff Category 3) and TCMR (Banff Category 4) and for the Combination of Non-TCMR (Banff Categories 2, 5, and 6)

	AUC	ACC	TPR	TNR	FPR	FNR	PPV	NPV	FDR	TP	TN	FP	FN
Elasticity (≤14.8 kPa) as a predictor for combination of borderline acute TCMR and TCMR	0.83	0.78	0.91	0.74	0.26	0.09	0.50	0.97	0.50	10	29	10	1
Dispersion (>15 m/s/kHz) as a predictor for combination of non TCMR	0.75	0.70	0.56	0.94	0.06	0.44	0.95	0.55	0.05	18	17	1	14

TCMR, T-cell mediated rejection; AUC, area under the receiver operating characteristic; ACC, accuracy; TPR, true positive rate; TNR, true negative rate; FPR, false positive rate; FNR, false negative rate; PPV, positive prediction value; NPV, negative prediction value, FDR, false discovery rate; TP, true positive; TN, true negative; FP, false positive; FN, false negative.

Table 4. Univariable and Multivariable Binary Logistic Regression to Identify Ultrasound Parameters for Predicting the Combination of Non-TCMR (Banff Categories 2, 5, and 6)

	Univariable analysis		Multivariable analysis	
	OR (95% CI)	*p* value	OR (95% CI)	*p* value
Age	1.017 (0.952–1.086)	0.623		
Sex	1.764 (0.531–5.865)	0.354		
Height	0.989 (0.918–1.065)	0.765		
Weight	0.972 (0.913–1.035)	0.378		
BMI	0.909 (0.733–1.128)	0.387		
Hypertension	0.318 (0.034–2.957)	0.314		
Diabetes mellitus	0.524 (0.161–1.700)	0.282		
Serum creatinine	1.106 (0.779–1.571)	0.573		
eGFR	1.001 (0.966–1.037)	0.969		
RI	4.709 (0.038–582.317)	0.528		
PI	2.010 (0.618–6.535)	0.246		
Vessel to capsule distance (Doppler)	1.264 (0.966–1.654)	0.087		
Vessel to capsule distance (SMI)	1.059 (0.577–1.943)	0.853		
SMI-VI	1.051 (0.964–1.146)	0.259		
Elasticity (kPa)	1.041 (0.974–1.112)	0.239		
IQR/median (elasticity)	75.208 (0.01–555541.6)	0.342		
Dispersion (m/s/kHz)	1.175 (1.019–1.355)	0.026	1.175 (1.019–1.355)	0.026
IQR/median (dispersion)	27.249 (0.071–10476.23)	0.276		
Graft length (cm)	1.774 (0.919–3.427)	0.088		
PT (mm)	0.969 (0.845–1.110)	0.645		
PSI	0.412 (0.092–1.843)	0.246		

TCMR, T-cell mediated rejection; OR, odds ratio; CI, confidence interval; BMI, body mass index; eGFR, estimated glomerular filtration rate; RI, resistance index; PI, pulsatility index; SMI-VI, superb microvascular imaging-vascular index; PT, parenchymal thickness; PSI, parenchyma size index.

learning models. Multiple performance metrics, including ACC, TPR, TNR, FPR, FNR, PPV, NPV, and FDR, for predicting the combination of non-TCMR categories are listed in Table 3.

DISCUSSION

In this study, we investigated the potential of multiparametric ultrasound parameters, especially 2D-SWE and 2D-SWD, as predictive factors for the combination of borderline acute TCMR and TCMR categories with a high NPV (0.97) and non-TCMR categories with a high PPV (0.95) in renal allografts with clinically suspected graft rejection, respectively. For predicting the combination of borderline acute TCMR and TCMR categories, as well as non-TCMR categories, the AUC values of elasticity (≤14.8 kPa) (0.83) and dispersion (>15.0 m/s/kHz) (0.75) were comparable to or higher than those of the machine-learning models, based on various clinical information. These results were based on univariate LR performed on the entire cohort of 50 patients, but similar outcomes were obtained when the analysis was repeated using 5-fold cross-validation.

Unlike native kidneys, allograft kidneys are typically located superficially in the iliac fossa. Therefore, recent studies have been conducted using various elasticity measurement methods, including real-time elastography,[22] transient elastography,[23] and acoustic radiation force impulse.[24] However, several confounding factors can affect the quantitative measurement of conventional elastography, including target depth, target

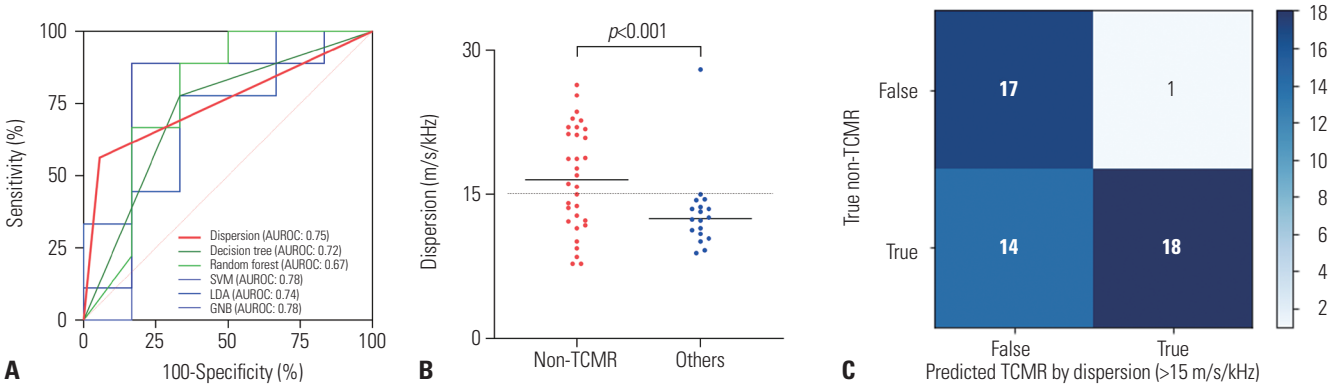

Fig. 5. (A) Receiver operating characteristic curves of dispersion (>15.0 m/s/kHz) and multiple binary classifiers for predicting the combination of non-TCMR (Banff category 2, 5, and 6). (B) A scatter plot for comparing the dispersion between the combination of non-TCMR (Banff category 2, 5, and 6) group, and the remaining groups. (C) Contingency matrix of dispersion (>15.0 m/s/kHz) and multiple binary classifiers for predicting the combination of non-TCMR (Banff category 2, 5, and 6). TCMR, T-cell mediated rejection.

movement, ROI area, transducer pressure, the incident angle of the acoustic beam, and the medium between the target and probe instruments or operator.[25] Therefore, in this study, we employed 2D-SWE, which is more accurate for evaluating liver fibrosis[26] and predicting renal allograft rejection.[27] 2D-SWE measures absolute organ stiffness and requires less stringent operational skills and experience.

Banff categories 2, 5, and 6, which are not related to TCMR, occur chronically and induce tissue fibrosis.[28] Previous studies have shown a positive correlation between the elasticity of the renal allograft cortex and histological fibrosis.[22,23,29-31] In this study, the combination of borderline acute TCMR and TCMR categories was more likely to occur during the acute period than in other groups (510 days vs. 2468 days) (Supplementary Table 2, only online). Moreover, the observed low elasticity (≤14.8 kPa) as a predictive cut-off value for the combination of borderline acute TCMR and TCMR categories, with a high NPV, seems consistent with the findings of previous studies. Controversies still exist regarding whether low elasticity indicates the subtype of the renal allograft. Kim, et al.[32] reported that a higher elasticity (31.0 kPa) indicated the presence of subclinical rejection (SCR) in stable functional renal allografts. However, this study was based on protocol biopsies taken 10 days and a year after kidney transplantation, rather than clinically suspected allograft rejection. Furthermore, the study investigated SCR rather than the histological subtypes of rejection. Therefore, comparing our findings with the results of this study in a parallel manner proves challenging.

Tissue viscosity differs from elasticity and is associated with the frequency dependence of the speed and attenuation of shear waves in the viscous component.[33] The 2D-SWD, implemented in clinical US systems (Aplio i800, Canon Medical Systems Corp. Otawara, Japan), along with 2D-SWE, has been reported to aid in diagnosing certain diffuse liver diseases[34] and transplanted livers;[35] however, no previous research has reported the association of 2D-SWD with the prediction of rejection subtypes in renal allografts. Sugimoto, et al.[36] reported that SWD was associated with inflammation in hepatic tissue in rat models, and Amioka, et al.[37] reported that tissue inflammation and SWD were associated with autoimmune myocarditis in rat models. An increasing body of evidence substantiates the link between tissue inflammation and SWD. Inflammatory changes, including necroinflammatory changes and tissue fibrosis, can increase dispersion.[35-37] The combination of non-TCMR likely has more tissue fibrosis compared to TCMR, which may explain the higher dispersion values observed. In light of these findings, additional research should be conducted to interpret the relatively high tissue dispersion (>15.0 m/s/kHz) observed in this study's non-TCMR categories.

This study had several limitations. First, the prospective study design could have inherently led to unavoidable selection bias, as we only included patients with clinically suspected renal allograft rejection. Second, since this was a single-center study, an external validation cohort was not available. Third, our analysis was based on a relatively small population of 50 renal allografts. Additional large-scale, well-designed diagnostic studies are needed to advance its clinical application. Fourth, the high hardware and software requirements for acquiring 2D-SWE and 2D-SWD images have necessitated the use of a single ultrasound equipment model for data acquisition. Therefore, additional validation utilizing diverse ultrasound equipment from multiple vendors is required. Finally, since renal allografts are located at a superficial layer beneath the skin, even minor pressure variations by the operator during probe placement can affect SWI results, potentially leading to high interobserver and intraobserver variations. Further validation using magnetic resonance elastography is required.

In conclusion, 2D-SWE and 2D-SWD are applicable as non-invasive predictive ultrasound parameters for the combination of acute TCMR and TCMR categories and non-TCMR categories in renal allografts with clinically suspected graft rejection. The AUC values of these parameters were comparable to or greater than those of the machine-learning models based on clinical information.

https://doi.org/10.3349/ymj.2024.0082

DATA AVAILABILITY STATEMENT

The data that support the findings of this study are available from the corresponding author upon reasonable request.

ACKNOWLEDGEMENTS

This study was supported by a research grant from Canon Medical Systems Korea (2021-CMSK-UL003).

AUTHOR CONTRIBUTIONS

Conceptualization: Jongjin Yoon, Dae Chul Jung, Young Taik Oh, and Kyunghwa Han. Data curation: Yeji Kwon, Dae Chul Jung, Young Taik Oh, and Byung Chul Kang. Formal analysis: Dae Chul Jung, Young Taik Oh, Kyunghwa Han, and Byung Chul Kang. Funding acquisition: Byung Chul Kang. Investigation: Dae Chul Jung, Young Taik Oh, Minsun Jung, and Byung Chul Kang. Methodology: Jongjin Yoon, Dae Chul Jung, Young Taik Oh, Kyunghwa Han, and Byung Chul Kang. Project administration: Byung Chul Kang. Resources: Jongjin Yoon. Software: Yeji Kwon, Jongjin Yoon, and Kyunghwa Han. Supervision: Byung Chul Kang. Validation: Yeji Kwon, Kyunghwa Han, and Byung Chul Kang. Visualization: Yeji Kwon. Writing—original draft: Yeji Kwon, and Jongjin Yoon. Writing—review & editing: Yeji Kwon, Jongjin Yoon, and Byung Chul Kang. Approval of final manuscript: all authors.

ORCID iDs

Yeji Kwon	https://orcid.org/0009-0000-5376-7270
Jongjin Yoon	https://orcid.org/0000-0003-4733-7658
Dae Chul Jung	https://orcid.org/0000-0001-5769-5083
Young Taik Oh	https://orcid.org/0000-0002-4438-8890
Kyunghwa Han	https://orcid.org/0000-0002-5687-7237
Minsun Jung	https://orcid.org/0000-0002-8701-4282
Byung Chul Kang	https://orcid.org/0000-0001-8939-3514

REFERENCES

1. Abecassis M, Bartlett ST, Collins AJ, Davis CL, Delmonico FL, Friedewald JJ, et al. Kidney transplantation as primary therapy for end-stage renal disease: a National Kidney Foundation/Kidney Disease Outcomes Quality Initiative (NKF/KDOQITM) conference. Clin J Am Soc Nephrol 2008;3:471-80.
2. Nankivell BJ, Kuypers DR. Diagnosis and prevention of chronic kidney allograft loss. Lancet 2011;378:1428-37.
3. Marcén R, Teruel JL. Patient outcomes after kidney allograft loss. Transplant Rev (Orlando) 2008;22:62-72.
4. Domański L, Kłoda K, Kwiatkowska E, Borowiecka E, Safranow K, Drozd A, et al. Effect of delayed graft function, acute rejection and chronic allograft dysfunction on kidney allograft telomere length in patients after transplantation: a prospective cohort study. BMC Nephrol 2015;16:23.
5. Preda A, Van Dijk LC, Van Oostaijen JA, Pattynama PM. Complication rate and diagnostic yield of 515 consecutive ultrasound-guided biopsies of renal allografts and native kidneys using a 14-gauge Biopty gun. Eur Radiol 2003;13:527-30.
6. Naesens M, Heylen L, Lerut E, Claes K, De Wever L, Claus F, et al. Intrarenal resistive index after renal transplantation. N Engl J Med 2013;369:1797-806.
7. Yang C, Jin Y, Wu S, Li L, Hu M, Xu M, et al. Prediction of renal allograft acute rejection using a novel non-invasive model based on acoustic radiation force impulse. Ultrasound Med Biol 2016;42:2167-79.
8. Gao J, Thai A, Erpelding T. Comparison of superb microvascular imaging to conventional color Doppler ultrasonography in depicting renal cortical microvasculature. Clin Imaging 2019;58:90-5.
9. Hai Y, Chong W, Liu JB, Forsberg F, Eisenbrey J. The diagnostic value of contrast-enhanced ultrasound for monitoring complications after kidney transplantation—a systematic review and meta-analysis. Acad Radiol 2021;28:1086-93.
10. Jeong HJ. Diagnosis of renal transplant rejection: Banff classification and beyond. Kidney Res Clin Pract 2020;39:17-31.
11. Sood P, Cherikh WS, Toll AE, Mehta RB, Hariharan S. Kidney allograft rejection: diagnosis and treatment practices in USA- A UNOS survey. Clin Transplant 2021;35:e14225.
12. Dietrich CF, Bamber J, Berzigotti A, Bota S, Cantisani V, Castera L, et al. EFSUMB guidelines and recommendations on the clinical use of liver ultrasound elastography, update 2017 (long version). Ultraschall Med 2017;38:e16-47.
13. Ferraioli G, Filice C, Castera L, Choi BI, Sporea I, Wilson SR, et al. WFUMB guidelines and recommendations for clinical use of ultrasound elastography: part 3: liver. Ultrasound Med Biol 2015;41:1161-79.
14. Loupy A, Haas M, Roufosse C, Naesens M, Adam B, Afrouzian M, et al. The Banff 2019 kidney meeting report (I): updates on and clarification of criteria for T cell- and antibody-mediated rejection. Am J Transplant 2020;20:2318-31.
15. Roufosse C, Simmonds N, Clahsen-van Groningen M, Haas M, Henriksen KJ, Horsfield C, et al. A 2018 reference guide to the Banff classification of renal allograft pathology. Transplantation 2018;102:1795-814.
16. Pareek J, Jacob J. Data compression and visualization using PCA and T-SNE. In: Goar V, Kuri M, Kumar R, Senjyu T, editors. Advances in information communication technology and computing. Singapore: Springer; 2021. p.327-37.
17. Pradhan B. A comparative study on the predictive ability of the decision tree, support vector machine and neuro-fuzzy models in landslide susceptibility mapping using GIS. Comput Geosci 2013;51:350-65.
18. Biau G. Analysis of a random forests model. J Mach Learn Res 2012;13:1063-95.
19. Chen HL, Yang B, Wang G, Wang SJ, Liu J, Liu DY. Support vector machine based diagnostic system for breast cancer using swarm intelligence. J Med Syst 2012;36:2505-19.
20. Xanthopoulos P, Pardalos PM, Trafalis TB. Linear discriminant analysis. In: Xanthopoulos P, Pardalos PM, Trafalis TB, editors. Robust data mining. New York: Springer; 2013. p.27-33.
21. Ontivero-Ortega M, Lage-Castellanos A, Valente G, Goebel R, Valdes-Sosa M. Fast Gaussian Naïve Bayes for searchlight classification analysis. Neuroimage 2017;163:471-9.
22. Orlacchio A, Chegai F, Del Giudice C, Anselmo A, Iaria G, Palmieri G, et al. Kidney transplant: usefulness of real-time elastography (RTE) in the diagnosis of graft interstitial fibrosis. Ultrasound Med Biol 2014;40:2564-72.
23. Nakao T, Ushigome H, Nakamura T, Harada S, Koshino K, Suzuki T, et al. Evaluation of renal allograft fibrosis by transient elastography (Fibro Scan). Transplant Proc 2015;47:640-3.
24. Lee J, Oh YT, Joo DJ, Ma BG, Lee AL, Lee JG, et al. Acoustic radiation force impulse measurement in renal transplantation: a prospective, longitudinal study with protocol biopsies. Medicine (Baltimore) 2015;94:e1590.
25. Shiina T, Nightingale KR, Palmeri ML, Hall TJ, Bamber JC, Barr

RG, et al. WFUMB guidelines and recommendations for clinical use of ultrasound elastography: part 1: basic principles and terminology. Ultrasound Med Biol 2015;41:1126-47.
26. Wu T, Wang P, Zhang T, Zheng J, Li S, Zeng J, et al. Comparison of two-dimensional shear wave elastography and real-time tissue elastography for assessing liver fibrosis in chronic hepatitis B. Dig Dis 2016;34:640-9.
27. Wang Z, Yang H, Suo C, Wei J, Tan R, Gu M. Application of ultrasound elastography for chronic allograft dysfunction in kidney transplantation. J Ultrasound Med 2017;36:1759-69.
28. Solez K, Colvin RB, Racusen LC, Haas M, Sis B, Mengel M, et al. Banff 07 classification of renal allograft pathology: updates and future directions. Am J Transplant 2008;8:753-60.
29. Gao J, Weitzel W, Rubin JM, Hamilton J, Lee J, Dadhania D, et al. Renal transplant elasticity ultrasound imaging: correlation between normalized strain and renal cortical fibrosis. Ultrasound Med Biol 2013;39:1536-42.
30. Arndt R, Schmidt S, Loddenkemper C, Grünbaum M, Zidek W, van der Giet M, et al. Noninvasive evaluation of renal allograft fibrosis by transient elastography--a pilot study. Transpl Int 2010;23:871-7.
31. Lukenda V, Mikolasevic I, Racki S, Jelic I, Stimac D, Orlic L. Transient elastography: a new noninvasive diagnostic tool for assessment of chronic allograft nephropathy. Int Urol Nephrol 2014;46:1435-40.
32. Kim BJ, Kim CK, Park JJ. Non-invasive evaluation of stable renal allograft function using point shear-wave elastography. Br J Radiol 2018;91:20170372.
33. Chen S, Urban MW, Pislaru C, Kinnick R, Greenleaf JF. Liver elasticity and viscosity quantification using shearwave dispersion ultrasound vibrometry (SDUV). Annu Int Conf IEEE Eng Med Biol Soc 2009;2009:2252-5.
34. Yoo J, Lee JM, Joo I, Lee DH, Yoon JH, Kang HJ, et al. Prospective validation of repeatability of shear wave dispersion imaging for evaluation of non-alcoholic fatty liver disease. Ultrasound Med Biol 2019;45:2688-96.
35. Lee DH, Lee JY, Bae JS, Yi NJ, Lee KW, Suh KS, et al. Shear-wave dispersion slope from US shear-wave elastography: detection of allograft damage after liver transplantation. Radiology 2019;293:327-33.
36. Sugimoto K, Moriyasu F, Oshiro H, Takeuchi H, Yoshimasu Y, Kasai Y, et al. Viscoelasticity measurement in rat livers using shear-wave US elastography. Ultrasound Med Biol 2018;44:2018-24.
37. Amioka N, Takaya Y, Nakamura K, Kondo M, Akazawa K, Ohno Y, et al. Impact of shear wave dispersion slope analysis for assessing the severity of myocarditis. Sci Rep 2022;12:8776.

https://doi.org/10.3349/ymj.2024.0082